Review | Received 2 October 2025; Revised 16 December 2025; Accepted 6 January 2026; Published 18 March 2026
https://doi.org/10.55092/neuroelectronics20260004

A review of wireless power and data transfer systems for biomedical implants

Binyao Hong[1,†], Xiao Wei[1,†], Chengyu Shi[1], Songping Mai[1,*], Xian Tang[1] and Zhihua Wang[1,2]

[1] Shenzhen International Graduate School, Tsinghua University, Shenzhen, China
[2] School of Integrated Circuits, Tsinghua University, Beijing, China

† These authors contributed equally to this work.

* Correspondence author; E-mail: mai.songping@sz.tsinghua.edu.cn.

Highlights:

- WPT: methods, principles & link optimization for mitigating PTE degradation.
- Innovative core circuit for WPDT systems.
- Challenges and future outlook for WPDT systems.

Abstract: This paper reviews recent research on wireless power and data transfer (WPDT) systems for implanted medical devices (IMDs). Focusing primarily on inductive WPDT systems, the review incorporates theoretical analyses and discussion of link optimization strategies. These strategies target power transfer efficiency (PTE) degradation caused by impedance mismatch, coil misalignment, inter-coil distance, and coupling angle-induced magnetic field inhomogeneity, summarizing referable solutions to mitigate such performance losses. The review also details key WPDT system components: in the power path, it covers power amplifiers, rectifiers, and voltage regulators; in the data path, it involves modulation schemes such as Amplitude-Shift Keying (ASK), Phase-Shift Keying (PSK), Frequency-Shift Keying (FSK), and Load-Shift Keying (LSK). Addressing the core challenge of balancing high PTE (typ. 50%) and data rate (typ. 0.1–2Mbps) under dynamic coupling and load variations, it summarizes the circuit innovation directions of each component, extending to integrated innovation paths at the system level. Finally, future directions are outlined, focusing on miniaturization, efficiency optimization via advanced circuits, biosafety, and robust modulation to enhance data reliability and speed, as well as the deep integration of machine learning for performance improvement.

Keywords: wireless power and data transfer; implanted medical devices; inductive WPDT systems; power transfer efficiency; link optimization; modulation schemes; system miniaturization

1. Introduction

In recent years, implanted medical devices have been widely applied in the medical field. IMDs can detect physiological parameters, stimulate affected sites, and exert therapeutic effects on various diseases, such

as cochlear implants to restore hearing for the deaf [1], cardiac pacemakers to regulate heart rhythm for patients with arrhythmia [2], spinal cord stimulators to alleviate chronic pain in the body [3], intraocular pressure sensors to monitor glaucoma progression in patients [4] and so on. However, packaged batteries are only capable of providing power to IMDs for a finite period, with this duration being jointly determined by the functional requirements of the IMDs and the battery's own capacity. Each battery replacement necessitates surgical intervention, posing safety hazards. Therefore, wireless power transfer (WPT) methods have been extensively developed to avoid surgery and thereby mitigate the risk of infection.

WPT refers to a power delivery method that transfers energy to implanted devices without physical contact, utilizing air or other material media as the transmission path. There are various methods of wireless power transfer, including electromagnetic coupling-based WPT, electromagnetic radiation-based WPT, and mechanical wave-based WPT.

Notably, IMDs require data reception and feedback for real-time monitoring to enable precise therapy, so a system that only transmits energy is insufficient, and it must transfer data simultaneously. Figure 1 depicts the basic configuration and components of a WPDT system. It incorporates a power path and an additional data path. For the power path, it contains transmitter (TX in Figure 1), wireless power link and receiver (RX in Figure 1), commonly consists of a power amplifier (PA), a couple of coils, a rectifier and a voltage regulator. Electric energy is output from the source to the PA and then transferred to the RX through the link coupled coils. The RX receives energy and outputs a stable voltage to the load through the rectifier and voltage regulator. For the data path, modulation techniques are employed to safeguard transmitted and received data from disturbances, demodulator is required to recover data.

PTE is the end-to-end efficiency that is the product of efficiencies of all power stages including PA (η_{PA}), coupling coils (η_{CC}), rectifiers (η_{REC}) and regulators (η_{REG}) [5]. PTE is the crucial indicator of the power path. When the system faces various changes such as coil coupling position or different loads, it is necessary to maintain high PTE. Data rate is the core indicator of the data path, representing the capability of data transmission. The transmission of data also affects the efficiency of power transfer [6]. Achieving high data rates while maintaining efficient energy transmission remains a key challenge for WPDT systems.

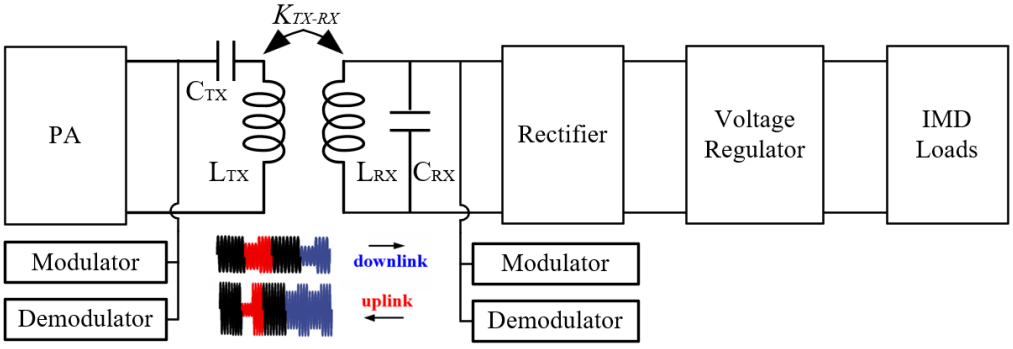

Figure 1. Basic structure of WPDT system for biomedical IMD.

This review systematically introduces the mainstream methods and core principles of wireless power transfer, and summarizes referable solutions for impedance mismatch and PTE degradation caused by magnetic field inhomogeneity resulting from coil misalignment, inter-coil distance, and

coupling angle in Section 2. Section 3 focuses on inductive WPDT systems, emphasizing the circuit implementation schemes of key components including power amplifiers, rectifiers, voltage regulators, modulation and demodulation modules in the WPDT system. Furthermore, it summarizes the circuit innovation directions of each module, and extends to the integrated innovation paths at the system level. The challenges and future outlook are summarized in Section 4. Section 5 concludes the review.

2.Wireless power transfer methods

Currently, WPT technologies are divided into three different types based on their core energy carriers and transmission principles. They are (1) electromagnetic coupling-based WPT, (2) electromagnetic radiation-based WPT, and (3) mechanical wave-based WPT.

2.1. Electromagnetic coupling-based WPT

This category relies on electromagnetic fields for energy transfer and mainly includes two sub-types: inductive power transfer (IPT) and capacitive power transfer (CPT).

2.1.1. Inductive power transfer

IPT mainly relies on the electromagnetic induction effect between the primary coil and the secondary coil. From the perspective of operating principles, IPT can be mainly categorized into the non-resonance IPT and resonant IPT. The schematic diagram of the non-resonance IPT system is shown in Figure 2.

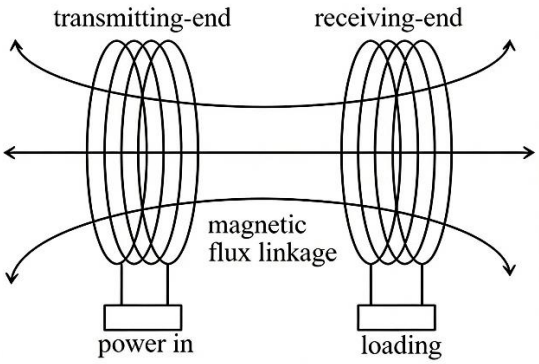

Figure 2. Non-resonance IPT system.

When the current passes through the transmitting coil, a magnetic field is generated around it. Two magnetically coupled coils create a mutual magnetic flux linkage. The mutual inductance coefficient from the transmitting coil to the receiving coil is defined as:

$$M_{RX\_TX} = \frac{\psi_{RX\_TX}}{i_{TX}} \quad (1)$$

here, ψ_{RX_TX} represents the mutual magnetic flux linkage between the transmitting and receiving coils, i_{TX} denotes the current flowing through the TX, and M_{RX_TX} signifies the mutual inductance between the two coils. Similarly, when a current i_{RX} flows through the RX, it induces a mutual magnetic flux linkage in the transmitting coil. The mutual inductance coefficient between two coils is defined as

$$M_{TX\_RX} = \frac{\psi_{TX\_RX}}{i_{RX}} \quad (2)$$

here, ψ_{TX_RX} denotes the mutual magnetic flux linkage between the transmitting and receiving coils, i_{RX} represents the current flowing through the receiving coil, and M_{TX_RX} indicates the mutual inductance from the transmitting coil to the receiving coil. Due to the reciprocity of mutual inductance between the two coils, it follows that

$$M_{RX\_TX} = M_{TX\_RX} = M \tag{3}$$

Considering the self-inductance effect of the coils themselves, the circuit equations between the transmitting coil and the receiving coil can be expressed as

$$u_{RX} = L_{RX}\frac{di_{RX}}{dt} + M\frac{di_{TX}}{dt} \tag{4}$$

$$u_{TX} = L_{TX}\frac{di_{TX}}{dt} + M\frac{di_{RX}}{dt} \tag{5}$$

Where u_{TX} represents the transmitting-end voltage, u_{RX} represents the receiving-end voltage, L_{TX} represents the inductance of the transmitting coil, L_{RX} represents the inductance of the receiving coil, i_{TX} represents the current inside the transmitting coil, and i_{RX} represents the current inside the receiving coil.

The schematic diagram of the resonant IPT system is shown in Figure 3. It consists of coupling coils and resonant caps.

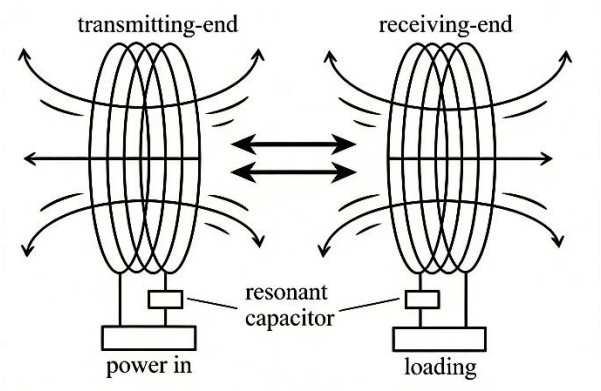

Figure 3. Electromagnetic resonance wireless power transfer system.

When the system is in resonance, the loop impedances of the transmitting-end inductive coil and the receiving-end inductive coil are expressed as follows

$$Z_1 = j\omega L_1 + \frac{1}{j\omega C_1} + R_1 \tag{6}$$

$$Z_2 = j\omega L_2 + \frac{1}{j\omega C_2} + R_2 \tag{7}$$

Where Z_1 represents the transmitting-end impedance, Z_2 represents the receiving-end impedance, L_1 represents the inductance of the transmitting-end coil, L_2 represents the inductance of the receiving-end coil, C_1 represents the transmitting-end resonant capacitor, C_2 represents the receiving-end resonant capacitor, R_1 denotes the internal resistance of the transmitter coil, R_2 denotes that of the receiver coil, and ω is resonant frequency. The equivalent impedance of the transmitting-end input is

$$Z_3 = Z_1 + (\omega M)^2 \frac{1}{Z_2 + R_L} \tag{8}$$

Where Z_3 represents the equivalent resistance of the transmitting-end input, Z_1 is the transmitting-end impedance, Z_2 is the receiving-end impedance, ω is the resonant frequency and R_L is the load resistance.

In a non-resonance IPT system, a small separation distance should be maintained between the primary and secondary coils, and precisely aligned to transfer energy effectively, acting as a tightly coupled air-core transformer [7]. The strict spatial positioning requirement limits its application in medical WPDT systems. In a resonance IPT system, however, efficient power transfer is still achievable even when the coils are loosely coupled, making resonant IPT a better choice for medical WPDT systems. Resonant frequencies are typically chosen from the ISM band, such as 6.78 MHz or 13.56 MHz [8], though this is not a strict requirement. The primary coil is driven by the PA to create magnetic flux, resulting in an induced AC voltage in the secondary coil. The secondary coil can be tuned to series-resonant or parallel-resonant configurations via resonant capacitors. The theoretical analysis above only covers the more widely used series-resonant structure. The choice between the 2 types of secondary tanks depends on the load conditions of the secondary circuit [9]. Generally, parallel-resonant is preferred for mW-range power transmission scenarios [10,11], while the series-resonant one is more advantageous for W-range power transmission [12]. However, in different medical WPDT systems, the specific resonant structure to use should be determined by the load conditions of the secondary coil. The output characteristics of the two resonant structures differ: the parallel-resonant secondary exhibits voltage-source characteristics, whereas the series-resonant secondary exhibits current-source characteristics [13]. The parallel-resonant configuration produces a distorted sinusoid at the output, while the series-resonant configuration maintains a sinusoidal output current. Different output characteristics affect the structure of the active rectifier used in the subsequent stage. From the primary side, the secondary appears as a reflected equivalent resistance. The overall reflected equivalent resistance is determined by the resonant structure, the corresponding active rectifier, and the subsequent load. According to the maximum power transfer principle, system PTE can be improved by maximizing this reflected equivalent resistance, thus requiring theoretical analysis of impedance matching to guide WPDT system design. The coupling coefficient k depends on the coils' geometry, distance, and alignment. For loosely coupled coils, k can be lower than 0.1 [14]. Larger transmission distances or lateral misalignments reduce coupling, leading to impedance mismatch and subsequent PTE degradation. Targeted efforts to address the misalignment problem will be discussed in the following sections.

Inductive WPT systems suffer from inherent problems, including a sharp drop in PTE induced by inter-coil displacement and impedance matching imbalance. Therefore, the optimization of the geometric shape of the coils along with the alternative fabrication materials, the construction of a multi-coil structure by additionally inserting coils for bridging to optimize impedance matching, and the optimization of the overall WPT link, have been involved in numerous works.

Planar coils can be utilized in either internal or external devices of WPDT systems. Based on the above fundamental principle of electromagnetic induction, in the context of implantable bioelectronics, a recent work focusing on optimizing the geometric shape of coils is proposed [15]. By utilizing S-parameter analysis, a unique systematic design approach for optimizing PTE (applicable to all transmitting and receiving coils) is put forward in [15]. It presents both theoretical and experimental test results, offering guidelines for the design of inductive implant links with spatial or area constraints. Resources related to inductive link optimization have been shared on GitHub by the authors.

To be specific, the design method in [15] is not restricted by the following conditions: (1) coupled coils can be symmetric or asymmetric; (2) the type and parameters of the impedance matching network (IMN) are unknown; (3) port impedances may be unequal. The trade-off between coil area and PTE is a critical design constraint for implantable systems. In general, the area of the transmitting coil is larger than that of the receiving coil to transmit more energy. Starting from the standard double-coil system, with the area of the receiving coil equal to that of the transmitting coil, a simplified theoretical analysis is presented in [15]. Due to the existence of intrinsic frequency, the optimum frequency and optimum inductance (L_{opt}) are determined by the constraints of coil design, and the coupling configuration of asymmetric transceiver coils is further introduced. Meanwhile, in addition to the structural optimization of double-coil configurations, dividing the coils into multiple parts and then recombining these parts in a certain way constitutes a new optimization strategy, which will be discussed in Section 2.2.1. This divide-and-merge method corresponds to multi-coil structures. Determining the optimum coil geometric shape is a prevalent challenge in WPDT. Planar spiral coils have various geometric shapes, such as circular, octagonal, hexagonal, and square ones.

After determining L_{opt}, the next step is to switch it into approximate physical geometry. For the planar spiral coil, targeted theoretical analysis is provided in [16]. L_{opt} can be formulated as follows.

$$L_{opt} = \frac{C_1 \mu_0 \mu_r n_j^2 d_{avg_j}}{2} \left[\ln\left(\frac{C_2}{\phi_j}\right) + C_3 \phi_j + C_4 \phi_j^2 \right] \tag{9}$$

Where, d_{avgj} is the average diameter, and φ_j is the filling ratio. The coefficients C_1, C_2, C_3, and C_4 are all defined by geometric shapes of coils. The coefficients mentioned above can be extracted from the models by EDA simulation software (HFSS) using finite element method (FEM) tools, and FEM is applicable to arbitrary geometric shapes. Different geometric shapes of coils exhibit distinct characteristics. In brief, for circular coils, the magnetic field is uniform and coupling robustness is strong, but space utilization is relatively low; for square coils, space utilization is high and manufacturing is simple; for the hexagonal, a good balance between magnetic field uniformity and space utilization; for octagonal ones, performance is close to that of circular ones. The specific choice of geometric shape should be determined by comprehensively considering room constraints and the series or parallel resonant topologies used. In general, many researchers prefer to use PCB coils with highly customizable shapes. Besides the commonly used rigid FR4 material, some flexible advanced materials are also employed for coils fabrication. The flexible packaging enables planar coils to be better applied in implantable systems. In [17], the planar coil of the implantable unit is fabricated using silver-plated copper conductors insulated with polyvinylidene fluoride. The coil, together with the PCB of the external control circuit, is used to build a complete implantable system. In [18], polydimethylsiloxane flexible packaging is used to fabricate *in vivo* implants and head-mounted components, while planar relay coils are manufactured on polyimide boards.

Misalignment between the RX and TX coils, along with inconsistencies in magnetic field uniformity induced by distinct coupling angles, can result in a marked decline in PTE. This represents a fundamental challenge that inductive WPDT systems are required to address. For example, in animal experiments, WPDT is adopted to eliminate the behavioral constraints imposed by wired connections, thereby minimizing stress to test subjects and enhancing the accuracy of experimental data. In medical WPDT applications, internal systems and external devices can also maintain stable data transmission while receiving power via coils, which reduces the sensitivity of PTE to distance. Accordingly, several targeted WPDT architectures, typically incorporating multi-coil configurations, have been proposed. These can be broadly

classified into 3 approaches, with 5 corresponding works taken as examples for illustration respectively. (1) The first topology involves arranging multiple TX coils in an omnidirectional layout [19–24]. This design enables the TX to deliver nearly uniform power regardless of the RX position and orientation. However, this approach requires increasing the size of TX coils, and system functionality depends on the mutual inductance between those multiple coils. The incorporation of multiple coils inevitably introduces additional complexity to the transmission system. (2) The second topology is based on a single TX coil, with RX coils arranged in an omnidirectional manner [25–28]. If the system is designed to generate a sufficiently strong magnetic field for WPDT, the TX power will be less affected by angular variations of the RX end. Increasing the number of coils, however, significantly increases the size and weight of the RX. (3) The third approach employs embedded coils or coil reconfiguration, such as anchor, butterfly, bowl type coils or sub-coils, 3-D antenna [29–31]. This approach facilitates the generation of a uniform magnetic field, even when the RX is positioned arbitrarily or subjected to rotational misalignment. However, the coils feature unique structures that pose significant manufacturing challenges, and there may be a considerable discrepancy between the fabricated coils and the electromagnetic simulation results.

For the first topology, in [19], a headstage and homecage based WPT system is proposed, which is applied in animal experiments for LED-optogenetic stimulation of mice. The system is generally composed of a transmitter, cage resonators, and a headstage module affixed to the animal's skull. The TX coil is positioned above the cage. Resonator coils are typically wound around the cage to establish a uniform magnetic field distribution within the entire volume. The modeling is shown in Figure 4. The TX (L1) is a double-layer coil with dimensions of 23.4 cm × 19.7 cm. The cage dimensions are 28.5 cm × 18 cm × 13 cm, allowing mice to move freely inside. Six single-turn coils (L2–L7) are used to wind around the cage for magnetic field generation, and the resonators operate at 13.26 MHz to augment the total magnetic flux and strengthen the coupling between the TX and RX coils. The measured results indicate that the PTE of the WPT system ranges from 34% to 42%. Multiple TX coils deliver power supply to the headstage module, while the resonators around the cage contribute to uniform power distribution across the entire cage volume. Similarly, a system designed for mouse medical experiments is proposed in [20]. This multi-EnerCage-Homecage system is improved from the EnerCage-HC and comprises multiple standard rodent cages. Each cage is wrapped with overlapping high Q-factor LC resonators fabricated from copper foil. The strong mutual coupling between these coils, in conjunction with their specific spatial arrangement, enables automatic magnetic field focusing onto the small headstage or implant, thereby covering the entire 3-dimensional volume within the cage. A closed-loop system is formed by multiple cages and TX coils driven by a Class-E PA operating at a resonant frequency of 13.56 MHz. Closed-loop power control guarantees that the headstage or implant receives the desired power, irrespective of misalignment caused by animal movement. WIFI and Bluetooth connections enable the PC-GUI to monitor multiple experimental subjects simultaneously. HFSS simulation results and measured power delivered to loads (PDL, ~60mW) show that the system reduces the sensitivity of the RX-side’s PDL to spatial position.

For the second topology, a reconfigurable-coil-array (RCA) is proposed in [25] to compensate for the drop in PTE caused by misalignment between coils in resonant WPT systems. By adjusting multiple variable capacitors of the coils to regulate the value of induced current in the coil array, the reconfiguration effect of coil size or shape can be achieved. A comparison was conducted between the traditional dual-coil WPT system and the proposed prototype WPT system with a reconfigurable coil array.

Measurements were conducted at 6.78 MHz for vertical distances of 10 mm and 30 mm, corresponding to 16.7% and 50% of the maximum coil dimension, respectively, in short- range and mid-range WPT system. For short-range operation, the system achieves a PTE exceeding 46.3% even under full misalignment (the Tx coil is completely shifted from the Rx coil). However, the PTE of the conventional dual-coil system degrades rapidly to 0% when misalignment exceeds 81.7%. In the midrange one, with 100% misalignment, the PTE of the traditional system is significantly enhanced from 6.8% to 37.1% following the incorporation of the proposed RCA. With a practical structure, the RCA serves as a viable solution to the misalignment problem. The coil has a length and width of approximately 60 mm, and the prototype holds potential for medical implantable WPDT applications.

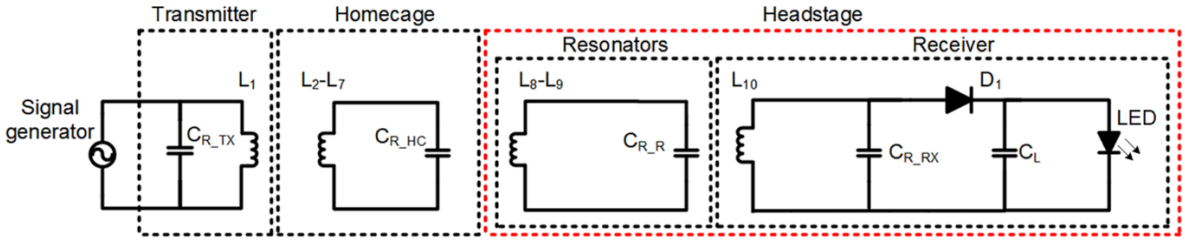

Figure 4. Equivalent modeling of the headstage and homecage based WPT system [19]. Reprinted with permission. Copyright 2020 IEEE.

For the last approach, a modified coil structure, consisting of multiple oppositely oriented sub-coils, is proposed in [29] for use as the TX end. This configuration maintains relatively constant coupling across a wide range of transmission distances. Microwave filters based on coupled resonators utilize 2 fundamental coupling mechanisms: electric and magnetic. The mutual cancellation of these two couplings results in a stable overall coupling coefficient across a wide range of distances [32]. Therefore, by determining the optimal coupling coefficient then allowing appropriate reverse currents to flow through the multiple sub-coils included in the modified TX coil, the sensitivity of PTE to misalignment can be reduced. This work provides theoretical analysis of the mathematical model and designs a prototype for measurement. In contrast to conventional dual-coil WPT systems, the proposed design maintains stable mutual inductance across varying distances and misalignments, thereby obviating the requirement for impedance tracking or active control circuits. The proposed TX coil has a maximum radius of 84.6 mm, with the RX coil being smaller in size. When the transmission distance d = 0–70 mm, a PTE of 88%–70% can be achieved; when the d = 40 mm and the misalignment ranges from 0–80 mm, a PTE of 85%–60% can be achieved. In [30], an anchor-shaped coil with a simple design, ease of fabrication, and planar structure is proposed. Derived from the loop antenna, this structure integrates a central bar element into the conventional loop antenna to yield dipole-like characteristics, while two notches are added to introduce an electrical coupling effect that strengthens the fringing field and thereby enables miniaturization of the antenna. Measurements and simulations were performed on the traditional loop antenna and the proposed anchor coil separately, with their diameters set to 9 cm or 15 cm. The results indicate that the PTE of the anchor-shaped coil is slightly lower than that of the loop antenna under small lateral misalignment scenarios, but it maintains more stable PTE across the full angular range. Therefore, in higher frequency scenarios than the conventional 13.56 MHz (e.g., 410 MHz), the prototype demonstrates advantages in PTE enhancement and robustness against coil misalignment and angular variations, thereby rendering it suitable for medical implantable systems.

The works corresponding to the above 3 methods provide reference solutions for the PTE degradation caused by coil position offset and magnetic field uniformity problems. Some are suitable for medical WPDT systems, while others are more applicable to animal experiments. For example, the multi-TX coil WPT system used in animal experiments in [19] would require constructing a massive "cage" if the experimental subject is switched from mice to human patients, resulting in high costs. In contrast, the approach in [29] that achieves insensitivity to offsets within the coil alignment range using sub-coils, and the modified coils similar to the planar special-shaped coil in [30], are more practically meaningful. Overall, considering the size constraints and power transfer requirements of medical WPDT systems, coil reconfiguration may have greater potential in addressing coil misalignment and enhancing PTE.

The rapid development of portable and implantable electronic devices has promoted extensive research on WPT methods. Coils are divided into two forms: the external and the implanted. The inductance of internally implanted coils is usually lower than that of external counterparts. In [33], the implanted coils are analyzed and optimized to achieve a high Q-factor. Besides the dual-coil structure, the multi-coil structure represents a new option for building WPT systems. It not only offers greater potential for achieving better impedance matching but is also employed to further explore link coupling modes, thereby enhancing PTE.

A WPT system constructed with a relatively traditional double-coil structure is introduced in [34]. It utilizes two parallel and opposing Helmholtz coils, which are specifically designed to power biomedical implants such as gastrointestinal capsules. Although the double-coil is a traditional transmission method, in recent years, many works related to WPT still adopt this transmission method to build systems.

A 6.78 MHz 3-coil WPT system, composed of a TX coil, a reconfigurable relay coil (RRC), and a RX coil, is introduced in [35]. Compared with the traditional 2-coil architecture, the addition of an RRC enables more effective impedance matching, significantly improving both transmission efficiency and load power compared to systems without impedance matching. In wireless power transfer, the load power delivered to the receiver-side resistor is affected by several factors, including changes in the coupling coefficient k caused by distance variations or lateral misalignment from the TX side, as well as the receiver-side RL and battery charge-levels. The frequency splitting behavior in the strong coupling region of the 3-coil system (TX coil, a relay coil, and RX coil) is deeply analyzed in [35], where the critical coupling boundary and impedance matching conditions are also derived. To maximize the efficiency of the transmitting end, a Class-D amplifier is utilized. For system feasibility verification only, a testbench is built but has not been truly applied to actual implantable devices.

Another 3-coil configuration featuring 2 TX coils and a single RX coil (excluding a relay coil) is presented in [36] for use in mouse brain stimulation experiments. The system exhibits insensitivity to changes in position and orientation, with improved performance achieved through the proposed crown-type 3-coil structure based on magnetically coupled resonant WPT. The coils are wound with copper wire to achieve miniaturization, allowing experimental mice to move freely while ensuring the chip works normally and generates stimulation signals for most of the time. According to the researchers' actual measurements, compared with the traditional 2-coil system, the proposed system can extend the experiment duration by approximately 7 times.

In addition to the aforementioned optimizations for coupled coils design, the entire system link can also be optimized. Machine learning (ML) is utilized to optimize the WPT link. In [37], the power supply

for the WPT system's Class-E PA is derived from a commercial Buck-Boost DC-DC converter (LTC3129, Analog Devices). The coil current and voltage are sampled and sent back to the microcontroller unit, which regulates the output voltage of the DC-DC to control the transmitted power: the greater the distance between the coils, the higher the transmitted power, and vice versa. Different coupling coefficients are set for the coils, and the transmitted power of the PA under different supply voltages is measured. The acquired dataset is utilized to train a backpropagation (BP) neural network, thereby developing a model that correlates coupling coefficients with transmitted power and facilitating the implementation of the closed-loop system.

In summary, for implantable WPT, energy is transferred through magnetic coupling between the TX and RX coils, where the latter is implanted inside the body. The strength of coils coupling directly affects WPT efficiency, and optimizing it is key to improving the wireless PTE. Multi-coils have relative advantages in impedance matching. Combined with the aforementioned coil-modification for coils misalignment problem, multi-coil configurations enable the WPDT systems to maintain high PTE over a large spatial range. When paired with a closed-loop system, this configuration helps enhance the stability of both energy and data transfer.

2.1.2. Capacitive power transfer

The CPT, as an emerging wireless power transfer method, uses two pairs of biocompatible insulating plates for energy transmission. The receiving plates can be made thin, suitable for implantable devices. In general, compared with traditional IPT, CPT usually operates at a higher frequency, while being smaller in size and SAR-friendly and EMI-friendly, making it a new option for building WPT systems. Low transmission distance, low PTE, and high sensitivity to tissue and environmental changes are disadvantages of CPT.

A summary of a CPT link intended for biomedical implants, along with methods (for tuned and uncompensated links) to optimize design for improved PTE, is offered in [38]. As shown in Figure 5, two different equivalent circuits share the same series-resonant link, corresponding to two kinds of CPT links: a tuned link that makes use of external inductors to eliminate parasitic capacitance, while the uncompensated link doesn't use external inductors. Compared with electromagnetic induction transmission, CPT links can enhance the power with load while maintaining biosecurity constraints (Electric-field, and specific absorption rate, SAR).

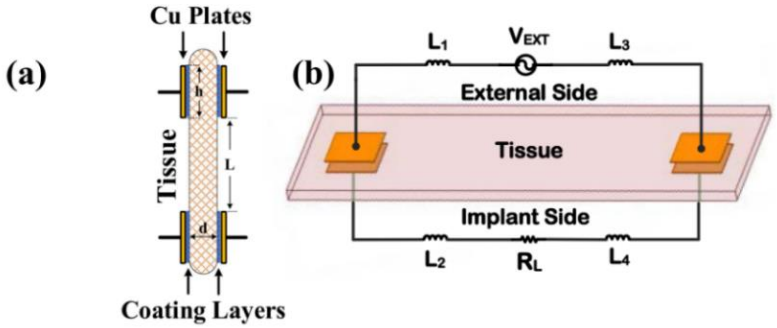

Figure 5. Equivalent circuit model of CPT link. **(a)** Cross-section, two pairs of coated Cu plates wrapped around body tissue (as dielectric); **(b)** Front view, series-resonant link driven by an external voltage source, delivering power to the implanted load [38]. Reprinted with permission. Copyright 2022 IEEE.

Another CPT design in [39], which uses parallel thin-film electrodes as coupling plates, employs resonant and non-resonant circuits to improve PTE and PDL. The optimization mechanism lies in reducing the impedance of insulating layer capacitors in the CPT link, effectively addressing the low PTE disadvantage of traditional CPT. Specifically, resonant circuits enhance energy transfer capability by using series inductors, while non-resonant circuits reduce CPT link impedance by increasing frequency.

2.2. Electromagnetic radiation-based WPT

This type of technology converts electrical energy to radio waves via a transmitter and propagates them, then a receiver turns waves to stable electricity for IMDs. Compared to IPT, electromagnetic radiation-based WPT has advantages like flexible transmission (no coil alignment), miniaturized receivers, and low electromagnetic interference. However, its transmission efficiency is very low, and this efficiency depends on the design of the antenna. Parameters like operating frequency, impedance bandwidth, and radiation pattern significantly impact the power received, making efficient antenna design essential to achieving effective power transfer [40].

To address the low PTE of IMD antennas, Ma *et al.* [41] proposed a combined receiving rectenna integrating a $30 \times 10 \times 0.456$ mm ^{3}magnetoelectric heterostructure antenna and a 60-turn $30 \times 12 \times 3$ mm ^{3} RF inductive coil (operating at 54 kHz). The magnetoelectric antenna's high-permeability Metglas focuses magnetic fields to boost coil inductance, while the coil provides a bias field enhancing magnetoelectric coupling. Simulations and measurements demonstrate that the combined antenna achieves a PTE of 2.82% at a distance of 15 mm from the TX coil, which is far higher than that of a single magnetoelectric antenna or a conventional coil. Similarly, Jing *et al.* [42] proposed a compact, circularly polarized implantable antenna operating at 2.4 GHz, which exhibits robust axial ratio and impedance bandwidths, and compact dimensions validated in human-mimicking materials. Zhang *et al.* [43] introduced a compact implantable rectenna for vascular devices, achieving miniaturization and notable conversion efficiency through optimized design.

2.3. Mechanical wave-based WPT

This type of technology uses mechanical waves as the energy carrier, and ultrasonic-based WPT (UWPT) is a typical representative. Electrical energy is converted into ultrasonic waves via transducers, after the ultrasonic waves propagate through solid or liquid media, they are converted back into electrical energy at the receiving end.

Ultrasonic waves exhibit efficient penetration through human soft tissues, possessing an energy attenuation rate significantly lower than that of electromagnetic waves. Furthermore, ultrasonic waves are free from electromagnetic interference (EMI), rendering them compatible with the sensitive electronic components utilized in implants. Although UWPT is highly sensitive to misalignment, its advantages make it suitable for powering implantable devices. And another limitation of UWPT is that this transmission method complicates the system design.

In [44], a hybrid magnetic-ultrasonic interrogation scheme is realized using a monolithic magnetoelectric transducer integrated within the implant. This transducer is capable of both generating and receiving magnetic fields and ultrasonic waves. The magnetoelectric transducer operates in two distinct modes (ultrasonic and magnetic field). By combining the advantages of these two modes, the

approach creates a favorable platform for millimeter-scale implants. Specifically, the platform can receive energy through one mode (either magnetic field or ultrasound) while using the other mode to transmit uplink data.

Similarly, in [45], ultrasonic waves are additionally employed to serve as the carrier for both energy and data transmission. This approach allows for precise and selective recording and stimulation of deep nerve fascicles. It features deep penetration, little influence from biological tissues, and no electromagnetic interference, making it suitable for implantable medical devices. For energy transmission, the full wave bulk-biased passive rectifier in the implant-integrated internal receiver converts the alternating current output by the ultrasound receiver into direct current.

Overall, IPT stands as the mainstream solution for IMDs. Relevant research addresses the degradation of PTE caused by misalignment through optimizing coil geometry, adopting multi-coil configurations, and introducing relay coils. Meanwhile, ML is integrated to optimize the link, enhancing stability and efficiency. CPT, as well as electromagnetic radiation-based and mechanical wave-based WPT, serve as supplementary technologies. Despite their respective limitations, they adapt to specific biomedical implant scenarios by virtue of their unique advantages, all three types of technologies focus on overcoming bottlenecks including transmission efficiency, size, and stability to meet application requirements.

3. Wireless power and data transfer systems

This section presents the basic concepts and innovation designs of each module in the power and data path, the innovation designs of WPDT systems will also be explained below.

3.1. Power path

The power path is responsible for transmitting the electrical energy from the external unit to the implanted device and providing a stable DC voltage for the IMD loads.

3.1.1. Power amplifier

At the energy-emitting terminal, a power amplifier is required to convert DC energy into amplified AC energy, which is then coupled to the secondary receiving terminal via a couple of coils. Traditional linear amplifiers have low efficiency and are not suitable in implantable medical devices; power amplifiers such as Class-D and Class-E, with an ideal efficiency of 100%, are needed as power-transmitting modules [46]. However, Class-E amplifiers rely on resonant networks, and their high load sensitivity makes it difficult to maintain high efficiency under wide-load conditions. In contrast, Class-D amplifiers, with lower load sensitivity, are widely used in wireless power transmission systems [47]. In order to improve the transmission efficiency and adapt to the changes in coil coupling and load conditions, the design of the PA should incorporate loss elimination and power adjustment technologies [48].

A Class-D PA with 1X/2X operation modes is proposed in [49]. By detecting the phase changes caused by load variations, the PA can switch between two modes to transmit different powers, thereby improving the system efficiency over a wide load range. A reconfigurable power amplifier is introduced in [50]. The PA is adjusted by the duty ratio of the control signal, which is tuned based on the load current, and the overall PTE is significantly improved by over 20%.

3.1.2. Rectifier

WPDT systems demand the conversion of AC input signals into unregulated DC signals. Rectifiers are employed to supply operating voltages for IMDs. Given the low power transmission efficiency inherent in magnetic or electromagnetic coupling mechanisms, the integration of high-efficiency and low-power-consumption rectifiers is critical for IMDs. This is primarily to mitigate device heating and the consequent risk of adjacent tissue damage induced by excessive power dissipation 0.Therefore, voltage conversion ratio (VCR) and power conversion efficiency (PCE) are key parameters for rectifiers. The relative displacement between the TX coil and the RX coil often leads to variations in the coupling condition, resulting in voltage fluctuations at the RX side [52], as depicted in Figure 6a.

Voltage-doubler (VD) is proposed to enhance the VCR and improve RX performance under variable link conditions. In [52], a single-stage dual-output regulating VD is proposed, which has a theoretical VCR of 2 and uses only one power transistor in each output path, optimizing the PCE-VCR trade-off in a single-stage dual-output RX structure. A dual-output regulating rectifier with VD topology is proposed in [53], which achieves a VCR twice that of the full-bridge topology and only requires 2 power transistors, thus saving on-chip area.

Traditional rectifiers with diodes suffer from large conduction voltage drops, resulting in low conversion efficiency. In contrast, active diodes controlled by comparators have lower conduction resistance and voltage drops, which are widely used in IMDs. A key challenge faced by active rectifiers, especially at high frequencies (such as 40.68 MHz, 13.56 MHz), is handling circuit delays (comparator delays, buffer delays). These delays will lead to a shortened switch conduction time, an increase in reverse current, and significant conduction losses of the body diode, all of which will reduce PCE and VCR. Various techniques have been adopted in the research to compensate for these delays and optimize the switching timing. Luo *et al.* [54] developed a 40.68 MHz active rectifier featuring a cycle-based delay compensation mechanism that dynamically tracks both turn-on and turn-off delays at each AC cycle. This mechanism utilizes internal delay cells and a ripple-based calibration loop to align the rectifier's timing edges with the zero-crossings of the input waveform, improving conduction window accuracy. Lee *et al.* [55] propose a 13.56 MHz active rectifier with a digital feedback-based adaptive delay control (DFDC) loop that optimizes both turn-on and turn-off switching timing. It combines analog comparators and envelope detectors by using fully digital delay logic and polarity detection circuits, significantly reducing area and power overhead. In [56], an adaptive delay-compensated active rectifier with 94.1% PCE is proposed, as shown in Figure 6b. This rectifier eliminates switching delays under PVT variations and device mismatches, ensuring stable high PCE.

Additionally, there are also researchers studying the regulation of rectifiers. This type of rectifier integrates rectification and voltage regulation functions into a single stage, eliminating the need for an independent voltage regulator, thereby potentially reducing cascade power losses. They can be designed with single output or dual output voltages. Eom *et al.* [57] presents a single-input multi-output resonant regulating rectifier capable of generating three distinct output voltages with 90.8% peak PCE to efficiently support multiple supply domains in implantable devices. A single-input dual-output (SIDO) rectifier that generates regulated output of 1.2 and 2.5 V is proposed in [50]. The measured maximum PTE at coil separation of 6 cm is 62.7%. A rectifier with sequential pulse frequency modulation control

is proposed in [58]. The rectifier outputs regulating voltages at 2.5 V and 3.3 V, each operating phase occupies an independent rectification cycle to avoid channel conduction problems.

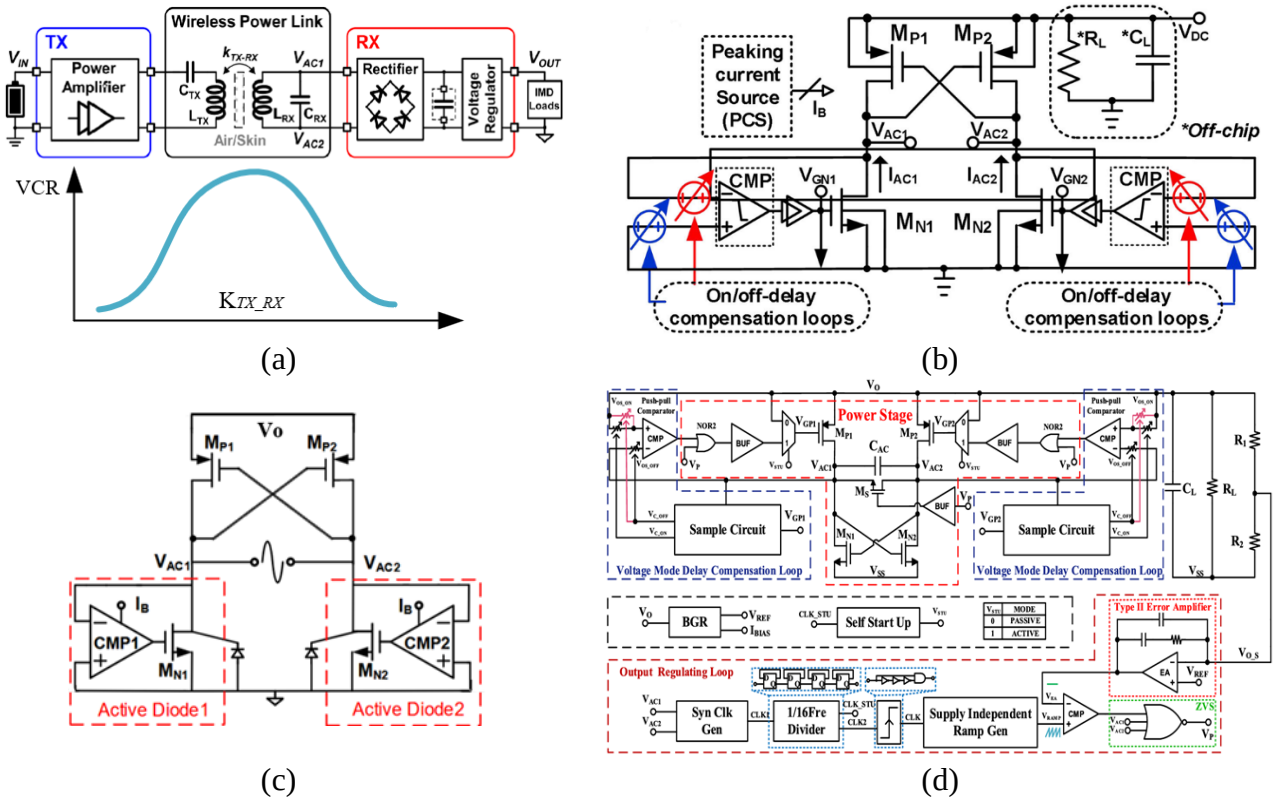

Figure 6. Variable VCR and innovative rectifier architecture. **(a)** VCR and V_{RX} change with the coupling conditions, different IMD loads require specific V_{RX} for power supply [52]. Reprinted with permission. Copyright 2024 IEEE.; **(b)** adaptive delay-compensated active rectifier [56]; **(c)** active rectifier; **(d)** The combination of PWM control mode and active rectifier enables single-stage voltage regulation and an improvement in VCR, an improved VM on-delay compensation method is proposed to address the large voltage pulse occurred on the RX [59].

3.1.3. Voltage regulator

The output voltage of rectifiers usually contains ripples and fluctuates with the AC input signal, thus requiring a voltage regulator to provide stable voltage for the electronic components in the subsequent modules. Commonly used regulators include Buck converters, Boost converters, and Low drop out (LDO) regulators. With a relatively simple circuit structure and few external components, LDO facilitates system integration and miniaturization, making it the preferred choice for medical implantable devices. Medical implantable devices feature sensitive circuits and variable loads with power supplies prone to noise, and LDO need high PSRR to suppress interference and fast transient response to maintain stable voltage [60]. Voltage regulators typically consist of three essential parts: (1) a reference generator, (2) an error amplifier, and (3) a power transistor [5]. The key performance indicators of LDO include linear regulation, load regulation, differential voltage, and power supply rejection ratio (PSRR). Among them, a good PSRR is particularly important for suppressing noise from the power supply, especially at higher frequencies.

In [61], a power supply ripple cancellation technique is proposed to improve the PSRR at high frequency. The proposed LDO achieves −71.8 dB of PSRR at 6.78 MHz and a 30 dB improvement in

PSRR at 126 MHz. In [62], the compensation capacitor cancels out the poles generated by the resistive feedback and broadens the loop bandwidth. With the input voltage of 1 V, the settling time is within 71.8 ns for a 50 mV overshoot and 63ns for a 47 mV undershoot. A load-tracking fast feedforward path for bandwidth extension is proposed in [63]. The LDO reaches a 38.5 MHz bandwidth with an active area of 0.0074 mm^2. In [64], an adaptive biasing, dynamic biasing technique is proposed to improve the load transient response, and a current mode feed-forward amplifier is used to compensate for the non-dominant pole. A 41 dB PSRR is achieved at 100kHz and the loop gain bandwidth product is 1.9 MHz.

In addition to the core voltage regulation function, the power management unit usually contains some auxiliary modules, which work closely with the voltage regulator to ensure the safe and stable operation of the system. A power feedback control unit is implemented in [65]. The system monitors the rectified voltage and regulates the delivered power within 20 μs by sending two control bits to the external unit through the inductive link.

3.2. Data path

IMDs require bidirectional data communication with external units, including downlink and uplink communications. Downlink communication is responsible for transmitting commands, parameters, and other data from the TX to the RX for controlling and configuring IMDs. It is achieved by modulating the wireless power carrier that supplies energy to the implant. Common modulation methods include ASK, PSK, and FSK, as shown in Figure 7. The implant receives the modulated signal and restores the original data through a demodulator. Uplink communication transmits physiological signals, device status, and other information from the RX to the TX, typically using LSK as the modulation method.

The data communication can generally be categorized into single-carrier transmission and multi-carrier transmission. Single-carrier transmission uses a set of coils to transmit energy and data simultaneously and enables straightforward implementation at the circuit and coil levels, ensures reliable data transmission, and contributes to the compactness of IMDs. However, it suffers from low data rate.

To achieve higher data rate, a multi carrier communication scheme independent of the power carrier is adopted. Typically, three separate coils are used for power supply, downlink and uplink data transmission, but this approach entails increased system design complexity and link interference risks. This section mainly focuses on single-carrier transmission, whose technical details and recent research will be introduced below.

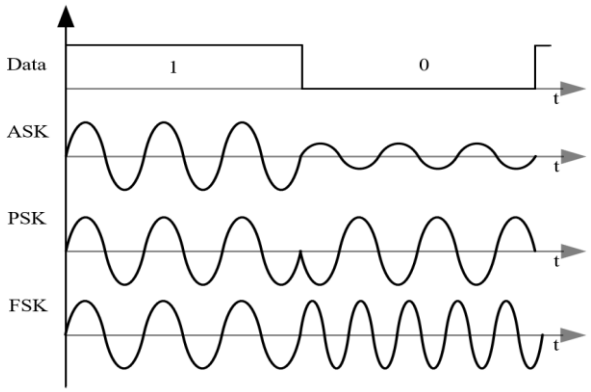

Figure 7. Modulation schemes. (1) ASK; (2) PSK; (3) FSK.

3.2.1. ASK

For ASK, signal transmission is achieved through amplitude modulation. The modulation and demodulation of ASK are characterized by straightforward implementation and low power consumption. Nevertheless, this modulation scheme is relatively susceptible to external perturbations, including noise, coupling fluctuations, and interference, these factors that can alter the carrier amplitude and thus result in low-rate data transmission [5]. The modulation depth (*MD*)) in ASK is defined as $MD = (V_H - V_L) / (V_H + V_L)$, where V_H denotes the maximum voltage amplitude and V_L represents the minimum voltage amplitude. Specifically, the ASK-modulated signal with 100% *MD* is referred to as On-Off Keying (OOK) amplitude modulation. Employing amplitude modulation schemes with low *MD* can reduce the interference of data communication on energy transmission [66], facilitating efficient and stable energy transfer. However, this approach also makes demodulation more challenging.

A novel ASK demodulator is proposed in [67]. Leveraging the switching characteristics of the core digital shaper under varied bias voltages, this structure enables a data rate of approximately 2.7 Mbps at 13.56 MHz. In [68], an envelope-detector-less (EDL) ASK demodulator is proposed, which replaces both the envelope detector and analog comparator in traditional ASK demodulators with a digital controller. With a silicon area of merely 0.023 mm^2, the EDL ASK demodulator can attain a maximum data rate of 500 kbps.

3.2.2. PSK

PSK encodes information by changing the phase of the carrier signal [69]. In binary PSK, 0 ° and 180 ° phases represent “0” and “1,” while higher-order versions like Quadrature PSK use multiple phases to transmit more bits per symbol. PSK can offer strong noise resistance, high spectral efficiency, and constant average power for efficient power amplification, but it requires strict carrier and phase synchronization at the receiver and has higher power consumption and complexity in design than ASK [70].

A multitone PSK modulation approach is introduced in [71]. This method demonstrates a reduction in voltage ripple at the diode output compared with ASK.

3.2.3. FSK

FSK conveys information by shifting the frequency of the carrier signal. In binary FSK, two distinct frequencies represent “0” and “1” [69]. FSK is less susceptible to amplitude-based noise, ensuring relatively stable data transmission, and its implementation is simple, reducing hardware complexity.

The basic structure of FSK demodulator is shown in [72], including a comparator to recover the clock, a frequency to voltage converter to convert the FSK clock into different voltages, and a hysteresis comparator to recover the data. An innovative three-tone FSK modulation technique is proposed in [73], which improves the PTE through waveform design without adversely affecting the transfer performance. The FSK modulation enhances the rectifier PCE by up to 9.04% and reduces the total harmonic distortion (THD) by 6.23%.

3.2.4. LSK

LSK is widely applied to transmit data from biological implantable devices to the outside of the body. It encodes digital information by altering the load impedance of the RX, which is reflected to the TX as a larger current amplitude change [73]. It demands minimal additional hardware components to implement and can also prevent the reduction of energy transmission efficiency during data transmission. However, LSK typically suffers from a low data rate. The process of changing load impedance has inherent speed limitations, which restricts the amount of data that can be transmitted in a given time frame. Additionally, LSK is quite vulnerable to environmental interference. External factors can easily disrupt the load impedance, causing signal distortion and potential data errors.

In [74], LSK data is transmitted by disrupting the resonant condition of the inductive link through controlling switches with off-chip capacitors. A maximum data rate of 0.678 Mbps is reached.

However, changing the resonant frequency for data transmission will reduce the amplitude of the signal received by IMDs and decrease PTE. Chen *et al.* [59] propose an LSK modulation circuit based on a dual-mode ramp generator. The rectifier switches between rectifier mode and VD mode, and the switching duty cycle loop is controlled by a PWM loop. It generates two types of ramp signals (increasing and decreasing) via the dual-mode ramp generator to encode the phase of PWM modulation, thereby integrating upstream data transmission into the mode switching of the voltage-stabilized rectifier and reducing the impact of the upstream data link on the power link.

3.2.5. Other modulation schemes

In addition to traditional modulation schemes, new modulation techniques have also been proposed. A novel modulation strategy is proposed in [75], which enhances the ratio of data rate to carrier frequency without significant degradation of power transfer efficiency. For a delivered load power of 32.3 mW and a data rate of 0.5 Mbps, the transmitter power efficiency reaches approximately 61%. Yao *et al.* [76] introduce a Delay-Shift Keying (DSK) technique for forward transmission through adjusting the deactivation time duration of the power amplifier, which enables voltage regulation while maintaining high PTE when transferring data.

3.3. Innovative WPDT systems and comparison table

Several innovative representative WPDT systems are introduced as follows. Table 1 provides a comparative review of the systems; the comparative indicators include modulation, CMOS technology, power link frequency, data rate, PCE, PTE, BER, and circuit area.

Huang *et al.* [56] proposed a high efficiency WPDT system, and the system architecture is shown in Figure 8. To resolve the trade-off between PTE and data rate, a frequency splitting inductive link operating in the strong coupling region is adopted, which extends the coil separation distance to 1.45 cm and ensures consistent link gain at dual carrier frequencies. An active rectifier integrated with adaptive delay compensation loops is adopted to minimize turn-on/off delays and reverse current loss, achieving a PCE of 94.1%. For low power demodulation, injection locked ring oscillators realize FSK to ASK conversion, and shifted limiters boost the modulation depth from 4.7% to 10.9%. The PTE of the

proposed design is 76.5%, the PDL is 40 mW, the data rate is 1.11Mbps, and this system exhibits excellent performance.

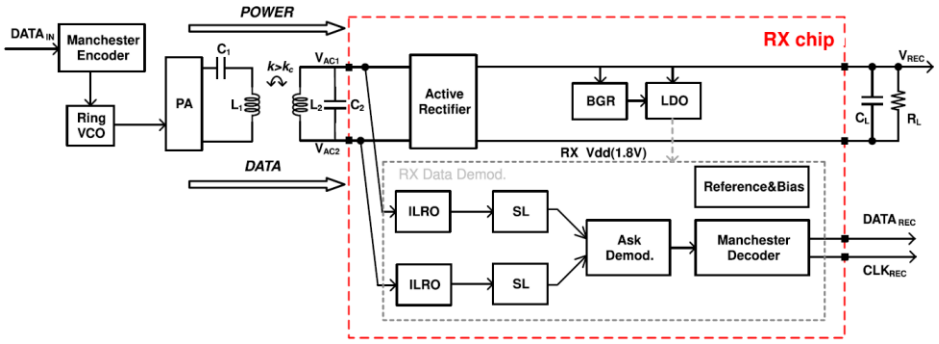

Figure 8. Overall architecture of the WPDT system [56].

Table 1. Comparation of the proposed WPDT systems.

Ref	Year	Tech (nm)	Link	Power	Downlink			Uplink			d	PCE	PTE	BER	PDL	Area
				f_{power}(MHz)	f_{down}(MHz)	Data(Mbps)	Modulation	f_{up}(MHz)	Data(Mbps)	Modulation	(mm)	(%)	(%)		(mW)	(mm^2)
[6]	2023	180	Single	13.56	-	-	-	13.56	1	ER-BT	10	83	-	<2.10E-06	-	2.50
[48]	2025	180	Single	13.56	13.56	-	LSK	-	-	-	12	92.4	54	-	145	7.81
[50]	2023	65	Single	13.56	-	-	-	13.56	0.423	LSK	20	88	50.8	<2.00E-05	20	0.58
[68]	2025	180	Single	2	2	0.5	ASK	-	-	-	10	-	36.1	<1.00E-02	92	0.52
[74]	2024	180	Multi	13.56/6.78	13.56/6.78	0.1	ASK	13.56/6.78	0.678	LSK	20	80.1	31.2	-	-	0.82
[76]	2024	180	Single	6.78	6.78	0.35	DSK	-	-	-	-	86.10	-	<1.000E-03	-	4.99
[77]	2025	180	Single	6.8/7.2	6.8/7.2	1	FSK	-	-	-	5	-	60.2	<1.00E-07	43.4	12.49
[78]	2022	180	Single	13.56	-	-	-	13.56	1	LSK	10	-	-	<9.10E-10	1.19	2.72
[79]	2022	180	Single	2	2	0.8	FSK	2	0.014	LSK	10	-	14	<3.12E-05	140	-
[80]	2021-	180	Single	6.5/7.5	6.5/7.5	2.5	FSK	-	-	-	5	-	56.7	<4.00E-07	115	2.32
[81]	2020	180	Single	10	10	1.66	CWM	-	-	-	10	-	30	<4.02E-07	29.7	3.25
[82]	2018	180	Single	13.56	13.56	0.21	PSK	13.56	0.105	LSK	10	81	48	-	54	25
[83]	2021	180	Single	13.56	13.56	0.34	PSK	13.56	0.34	LSK	8	73.7	-	-	50	12.00
[84]	2025	180	Multi	4/5	4/5	0.25	FSK	-	0.067	LSK	5	-	49	<1.00E-06	120	2.85

Traditional WPDT systems suffer from issues such as significant energy loss in short-coil back telemetry (SC-BT) and the inability to perform forward telemetry (FT) during BT operations. To tackle these issues, Kim *et al.* proposed a 13.56 MHz WPDT system integrating current-modulated energy-reuse back telemetry (ER-BT) and an energy-adaptive dual-input LDO [6]. The conceptual block diagram of the WPDT system is shown in Figure 9. The ER-BT employs current modulators to draw instantaneous current from the secondary coil during BT, storing the energy in a storage capacitor instead of dissipating it; this stored energy is then boosted and reused through the dual-input LDO, which adaptively combines energy from the rectifier and the stored BT energy to supply the load. Additionally, an active rectifier is incorporated to minimize power losses by optimizing switching and conduction losses. The system achieves a maximum BT data rate of 1 Mb/s, reduces energy consumption by as much as 42% in comparison with SC-BT at an input power of 3.05 mW, and enables FT demodulation during BT operations.

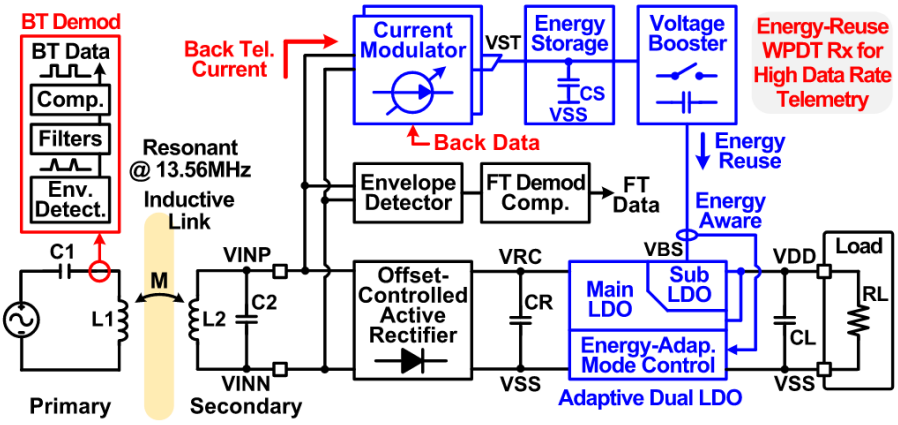

Figure 9. Overall block diagram of the WPDT system with the proposed ER-BT [6]. Reprinted with permission. Copyright 2023 IEEE.

Karimi *et al.* [74] propose a WPDT system leveraging a single inductive link with dual-band coils and frequency-division multiple access to enable independent powering and communication with each implant. The schematic diagram of proposed WPDT system is illustrated in Figure 10. It integrates a digitally aided active rectifier with latch-based comparators to reduce delay time, achieving a 90.2% VCR and 80.1% PCE. A voltage reference outputs 1.2 V, which powers the implant and serves as a reference for other modules. A LDO has been designed to deliver a 1.8 V supply voltage to other components, thus enabling power supply to multiple implants. A power control unit ensures safe operation through feedback mechanisms (with a 2–2.45 V control range), a power-on-reset function (triggering at 1.75 V), and a voltage limiter (activating at 3.53 V). For data transmission, bidirectional half-duplex communication is supported via ASK modulation for downlink using a self-sampling separated-biasing demodulator, while LSK modulation is utilized for uplink transmission by adjusting the load of the LC resonant tank. The achieved data rates are 0.678 Mbps and 0.1 Mbps for downlink and uplink respectively, with a bit error rate lower than 10^{-6}.

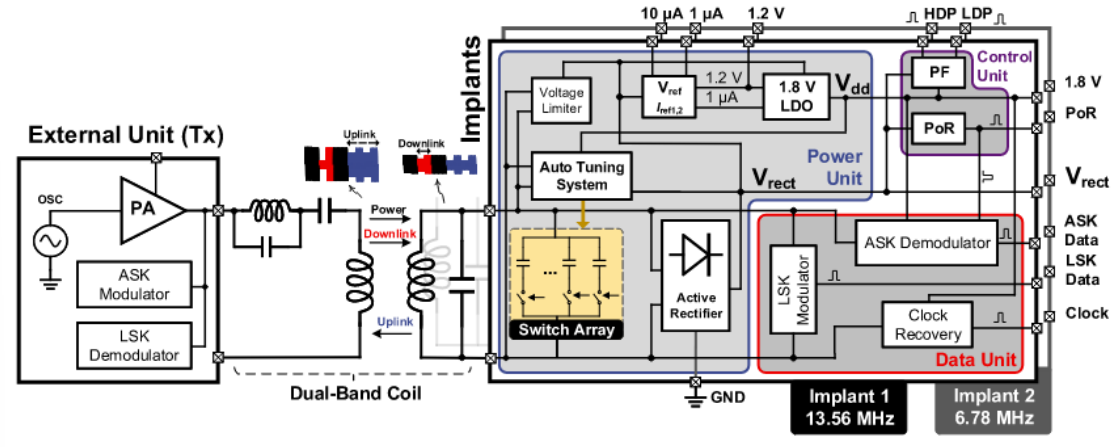

Figure 10. Block diagram of WPDT system with global power control for the closed-loop IMDs [74]. Reprinted with permission. Copyright 2024 IEEE.

In summary, this section focuses on the core composition and innovative directions of WPDT systems, systematically elaborating on the key technologies of the power path, data path, and system level integration schemes. For the power path, technologies such as reconfigurable topologies, delay

compensation, high-efficiency voltage regulation, and feedback control are adopted to optimize energy transfer efficiency and output stability, adapting to dynamic coupling and load variation scenarios. The data path is based on classic modulation scheme, balancing low power consumption, anti-interference performance, and data rate requirements, while exploring emerging modulation technologies like DSK to further enhance bidirectional communication performance. System level innovations cover SIDO architectures, energy-reuse back telemetry and dual-band coil designs, achieving a dynamic balance between PTE, data rate, and system miniaturization. These technological innovations and integration schemes provide critical technical support for IMDs.

4. Challenges and future outlook

The core challenges in the field of biomedical implant wireless power transfer and data communication lie in achieving high miniaturization and improving overall system power efficiency. Simultaneously, strict adherence to bio-safety standards is paramount. Furthermore, ensuring reliable and efficient bidirectional data communication capability in dynamic biological environments is a critical task.

To address these challenges, future optimization directions will primarily focus on enhancing the balance between size and efficiency, with research continuing to explore smaller receiver coil and transducer designs—for example, successful implementations include a 4 mm diameter receiver coil [54] and a 9.5 mm ultra-miniature receiver coil [77], along with $5 \times 2 \times 0.2$ mm magnetoelectric transducers [85], all tailored to meet minimally invasive implantation requirements. Concurrently, advanced circuit designs such as adaptive rectifiers utilizing cycle-based timing control [54] or DFDC [55], coupled with dynamic voltage supply [55] techniques and optimized power management units, will be crucial for achieving higher PTE and extended device lifespan.

WPDT systems confront core safety challenges including tissue heating, SAR limits, and biocompatible encapsulation. Tissue heating arises from the deposition of electromagnetic energy in biological tissues, potentially causing burns or abnormal stimulation. Moreover, the constraints imposed by SAR limits on transmission power exacerbate the dilemma of balancing efficiency and safety [86]. In [87], a near-field deep tissue transmission system based on a slot antenna array can overcome transmission distance limitations, yet high-frequency electromagnetic radiation tends to accumulate in deep tissues, leading to local temperature elevation and the risk of exceeding SAR thresholds. A circularly polarized implantable antenna operating in the 915 MHz ISM band exhibits a SAR value of 0.17 W/kg over 1 gram of tissue [88], which complies with standards, but increasing transmission gain may cause power to exceed SAR limits. A dual-band implantable rectenna system achieves power conversion efficiencies of 79.9% (0.915 GHz) and 72.8% (2.45 GHz) [89]; however, individual variations in the dielectric properties of human tissues can induce fluctuations in SAR values, increasing the uncertainty of tissue heating. Meanwhile, the packaging of implants must achieve a precise balance between electrical conductivity, *in vivo* stability, and biosafety. Firstly, packaging must adapt to the physiological environment of the implantation site. The hydrogel-based intraocular pressure monitoring sensor developed by Xu *et al.* [90], which is in direct contact with the inner eyelid, requires its packaging materials to balance wireless signal penetration and tissue comfort, making the biocompatible replacement of conductive materials a core challenge. Secondly, the biological stability of packaging is insufficient for long-term implantation scenarios. In [91], although the proposed bioresorbable intracranial pressure (ICP) monitoring sensor avoids the risk of secondary surgery, its packaging

materials must maintain structural integrity in the body for an extended period to ensure reliable data transmission. Thirdly, there is a prominent contradiction between flexible packaging and functional integration. While the implantable ICP monitoring antenna based on a polyimide (PI) substrate [92] achieves complex circuit integration by virtue of PI's excellent thermal stability, the substrate's limited flexibility makes it difficult to adapt to the deformation of *in vivo* tissues after packaging, easily leading to damage to the packaging layer and signal attenuation.

Developing systems with high tolerance to implant position and orientation changes is also vital, exemplified by proposals for three-dimensional resonant current-mode wireless receivers that enable real-time link adaptivity to ensure stable charging irrespective of position, angle, or time variations [93]. Notably, magnetoelectric transducers themselves also exhibit tolerance to angular offset [85]. Furthermore, data communication reliability and speed will see significant advancements through the integration of more robust and low-power modulation and demodulation schemes, including ASK, which is widely adopted for low-power implants and has recent demodulator designs achieving data rates up to 2.7 Mbps at low power consumption [67] and supporting ultra-low modulation depths as low as 0.03% [66]. FSK and PSK are being explored to optimize the trade-off between power transfer efficiency and data rate. PWM is also being applied to data transmission [59], particularly when combined with magnetoelectric transducers, facilitating efficient backscatter communication with demonstrated data rates of 17.73 kbps [85]. Key technologies for enhancing performance also include DSK for downlink communication [76], which enables simultaneous voltage regulation without affecting efficiency. In terms of achieved data rates, current systems demonstrate uplink speeds of 423.75 kb/s [50] and downlink speeds of up to 1 Mb/s [77]. Efficient backscatter communication technologies like LSK remain a crucial direction for improving uplink performance.

In recent years, ML has been increasingly deeply integrated with WPDT systems. ML algorithms are capable of optimizing the geometric and structural configurations of WPT coils, forecasting the optimal parameter combinations of inductive couplers, and improving the coupling efficiency in dynamic operating environments. In addition to these performance-oriented optimizations, ML techniques are also applied to foreign object detection (FOD) systems, where they identify interfering metallic and biological objects to safeguard the stability and safety of power transmission processes. In terms of geometric and structural design optimization, the combination of neural networks and meta-heuristic algorithms directly predicts power transfer efficiency by training on 35,000 sets of Finite Element Method simulation data, reducing the coil optimization time from months to seconds [94]. A convolutional neural network (CNN) based model can convert magnetic field intensity into grayscale images to quickly predict optimal coil parameters, shortening the optimization time from 23.74 s to 3.2 ms [95]. For the prediction of inductive coupler parameters, a feedforward neural network establishes a mapping relationship between equivalent load impedance and optimal matching capacitor values by learning 220 datasets, dynamically selecting the optimal transmitting coil and increasing the coupling efficiency to 95% [96]. In terms of coupling efficiency optimization, the synergy of CNN and Particle Swarm Optimization completes the localization of the receiver coil's position and orientation within 731.86 μs, compensates for misalignment losses through magnetic beamforming, and simultaneously controls the SAR within a safe range [97]. A backpropagation neural network learns the mapping relationship of coupling coefficients through the voltage and current data at the transmitting end, dynamically adjusting the supply voltage of the Class-E power amplifier to maintain stable coupling within a transmission distance of 18 mm [98].

In FOD detection, neural networks, Support Vector Machines and other algorithms accurately identify metallic foreign objects such as empty aluminum cans by analyzing input impedance trajectories in the 75–85 kHz frequency band, achieving a classification efficiency of 85%–100% [99]. YOLOv4 and its lightweight version realize real-time detection of foreign objects on the surface of charging pads by training FOD datasets through transfer learning, with an average precision of over 97.74%, effectively avoiding interference risks [100]. These applications significantly break through the computational bottlenecks and adaptability limitations of traditional methods by mining nonlinear relationships in data, providing technical support for addressing challenges such as coil alignment, high efficiency and safety of WPT systems.

In summary, the core challenges of WPDT systems focus on miniaturization, high PTE, biosafety, and reliability of bidirectional data communication in dynamic environments. Future optimizations will center on hardware miniaturization and circuit design upgrades to improve PTE, strengthen safety and robustness through thermal management and packaging material optimization, and improve data communication performance by leveraging low-power modulation and demodulation technologies. The deep integration of machine learning will provide efficient solutions for coil design optimization, parameter prediction, misalignment compensation, and FOD, further promoting the evolution of WPDT systems toward a more efficient, safe, and intelligent paradigm.

5. Conclusion

The review focuses on WPDT systems, conducting a systematic collation targeting the link optimization of IPT, the implementation and innovation of WPDT system circuits in recent years, as well as the core challenges and future outlooks of WPDT systems.

In terms of IPT link optimization, the review collates solutions to address PTE degradation caused by impedance mismatch, coil misalignment, and magnetic field inhomogeneity, including coil geometric and material optimization, multi-coil configurations, relay coil introduction. Additionally, the integration of ML algorithms for link optimization has emerged as a promising approach, enabling dynamic adjustment of system parameters to compensate for misalignment and load variations, thereby improving the stability and efficiency of power transfer.

For circuit implementation and innovation, the review elaborates on technological advancements in the power path (PA, rectifiers, voltage regulators) and data path (modulation and demodulation schemes such as ASK, PSK, FSK, LSK, DSK). System level innovations like SIDO architectures and energy-reuse back telemetry achieve a dynamic balance between PTE, data rate, and miniaturization, providing solid technical support for IMDs.

Additionally, the review identifies core challenges including miniaturization, high PTE, biosafety, and reliable bidirectional data communication. Future directions will focus on miniature component design, advanced circuit optimization, biosafety enhancement through packaging and thermal management, and deep integration of ML for coil design, parameter prediction, and misalignment compensation.

Data availability statement

No new data were created or analyzed in this study.

Declaration of generative AI and AI-assisted technologies

During the preparation of this manuscript, the authors used generative AI tools only to improve language and readability. The authors take full responsibility for the content of the manuscript.

Acknowledgments

This work was supported by the Shenzhen Science and Technology Innovation Bureau under Grant No. KJZD20240903103159001.

Authors' contribution

Conceptualization, Songping Mai; methodology, Xian Tang; investigation, Binyao Hong and Xiao Wei; data curation, Binyao Hong and Xiao Wei; writing—original draft preparation, Binyao Hong, Xiao Wei and Chengyu Shi; writing—review and editing, Binyao Hong and Xiao Wei; visualization, Binyao Hong and Xiao Wei; supervision, Songping Mai; project administration, Zhihua Wang. All authors have read and agreed to the published version of the manuscript.

Conflicts of interest

Zhihua Wang holds the position of Associate Editor for *Neuroelectronics* and has not peer reviewed or made any editorial decisions for this paper.

References

[1] Kipping D, Zhang Y, Nogueira W. A computational model of the electrically or acoustically evoked compound action potential in cochlear implant users with residual hearing. *IEEE Trans. Biomed. Eng.* 2024, 71:3192–3203.

[2] Wang Y, Zhang C, Zheng C, Jin H, Zhang G, *et al.* A 590-nA fully-integrated AFE including a CSCCIA with SC ripple rejection and a configurable SC-BPF for implantable cardiac pacemakers. In *2024 IEEE Biomedical Circuits and Systems Conference (BioCAS)*, Xi'an, China, October 24–26, 2024, pp. 1–5.

[3] Yang CC, Ker MD. Miniaturized wirelessly-powered biphasic current stimulator for implantable neurostimulation. In *2025 IEEE International Symposium on Circuits and Systems (ISCAS)*, London, UK, May 25–28, 2025, pp. 1–5.

[4] Lan Z, Shi J, Hao J, Wang Z, Guo Y, *et al.* A fully-integrated 0.068-mm^3 implantable pressure sensing device with wireless energy harvesting and data telemetry. *IEEE Trans. Biomed. Circuits Syst.* 2025, pp. 1–12.

[5] Karimi MJ, Schmid A, Dehollain C. Wireless power and data transmission for implanted devices via inductive links: a systematic review. *IEEE Sens. J.* 2021, 21(6):7145–7161.

[6] Kim M, Lee HS, Ahn J, Lee HM. A 13.56-MHz wireless power and data transfer system with current-modulated energy-reuse back telemetry and energy-adaptive voltage regulation. *IEEE J. Solid-State Circuits* 2023, 58(2):400–410.

[7] Cheng L, Ki WH, Lu Y, Yim TS. Adaptive on/off delay-compensated active rectifiers for wireless power transfer systems. *IEEE J. Solid-State Circuits* 2016, 51(3):712–723.

[8] Riehl PS, Satyamoorthy A, Akram H, Yen YC, Yang JC, *et al.*, Wireless power systems for mobile devices supporting inductive and resonant operating modes. *IEEE Trans. Microwave Theory Tech.* 2015, 63(3):780–790.

[9] Wang CS, Covic GA, Stielau OH. Power transfer capability and bifurcation phenomena of loosely coupled inductive power transfer systems. *IEEE Trans. Ind. Electron.* 2004, 51(1):148–157.

[10] Li X, Tsui CY, Ki WH. A 13.56 MHz wireless power transfer system with reconfigurable resonant regulating rectifier and wireless power control for implantable medical devices. *IEEE J. Solid-State Circuits* 2015, 50(4):978–989.

[11] Lee HM, Ghovanloo M. An Integrated Power-efficient active rectifier with offset-controlled high speed comparators for inductively powered applications. *IEEE Trans. Circuits Syst. I Regul. Pap.* 2011, 58(8):1749–1760.

[12] Choi JH, Yeo SK, Park S, Lee JS, Cho GH. Resonant Regulating Rectifiers (3R) operating for 6.78 MHz Resonant Wireless Power Transfer (RWPT). *IEEE J. Solid-State Circuits* 2013, 48(12):2989–3001.

[13] Schuylenbergh KV, Puers R. *Inductive Powering-Basic Theory and Application to Biomedical Systems*. New York: Springer, 2009.

[14] Nadakuduti J, Lu L, Guckian P. Operating frequency selection for loosely coupled wireless power transfer systems with respect to RF emissions and RF exposure requirements. In *2013 IEEE Wireless Power Transfer (WPT)*, Perugia, Italy, 2013, pp. 234–237.

[15] Omi AI, Jiang A, Chatterjee B. Efficient inductive link design: a systematic method for optimum biomedical wireless power transfer in area-constrained implants. *IEEE Trans. Biomed. Circuits Syst.* 2025, 19(2):300–316.

[16] Mohan SS, Hershenson MM, Boyd SP, Lee TH. Simple accurate expressions for planar spiral inductances. *IEEE J. Solid-State Circuits* 1999, 34(10):1419–1424.

[17] Gour N, Ehsani A, Javan-Khoshkholgh A. A batteryless implantable system with adaptive near-field communication to study neurogastroenterological disorders. In *2024 46th Annual International Conference of the IEEE Engineering in Medicine and Biology Society (EMBC)*, Orlando, USA, July 15–19, 2024, pp. 1–4.

[18] Lee J, Leung V, Lee AH, Huang J, Asbeck P, *et al.* Neural recording and stimulation using wireless networks of microimplants. *Nat. Electron.* 2021, 4:604–614.

[19] Biswas DK, Martinez JHA, Daniels J, Bendapudi A, Mahbub I. A novel 3-D printed headstage and homecage based WPT system for long-term behavior study of freely moving animals. In *2020 IEEE Radio and Wireless Symposium (RWS)*, San Antonio, USA, January 26–29, 2020, pp. 268–271.

[20] Mirbozorgi SA, Jia Y, Zhang P, Ghovanloo M. Toward a high-throughput wireless smart arena for behavioral experiments on small animals. *IEEE Trans. Biomed. Eng.* 2020, 67(8):2359–2369.

[21] Sergkei K, Lombard P, Semet V, Allard B, Moguedet M, *et al.* The Potential of 3D-MID technology for omnidirectional inductive wireless power transfer. In *2018 13th International Congress Molded Interconnect Devices (MID)*, Würzburg, Germany, September 25–26, 2018, pp. 1–6.

[22] Chow JPW, Chung HSH, Chan LLH, Shen R, Tang SC. Optimal design and experimental assessment of a wireless power transfer system for home-cage monitoring. *IEEE Trans. Power Electron.* 2019, 34(10):9779–9793.

[23] Mirbozorgi SA, Jia Y, Canales D, Ghovanloo M. A wirelessly-powered homecage with segmented copper foils and closed-loop power control. *IEEE Trans. Biomed. Circuits Syst.* 2016, 10(5):979–989.

[24] Narayanamoorthi R, Juliet AV. IoT-enabled home cage with three-dimensional resonant wireless power and data transfer scheme for freely moving animal. *IEEE Sens. J.* 2018, 18(19):8154–8161.

[25] Lim T, Lee Y. Reconfigurable coil array for near-field beamforming to compensate for misalignment in WPT systems. IEEE Trans. Microwave Theory Tech. 2021, 69(11):4711–4719.

[26] Lenaerts B, Puers R. Inductive powering of a freely moving system. *Sens. Actuator A Phys.* 2005, 123:522–530.

[27] Jia Y, Mirbozorgi SA, Wang Z, Hsu CC, Madsen TE, et al. Position and orientation insensitive wireless power transmission for EnerCage-Homecage system. *IEEE Trans. Biomed. Eng.* 2017, 64(10):2439–2449.

[28] Ryu M, Kim JD, Chin HU, Kim J, Song SY. Three-dimensional power receiver for in vivo robotic capsules. *Med. Biol. Eng. Comput.* 2007, 45(10):997–1002.

[29] Zhuang Y, Chen A, Xu C, Huang Y, Zhao H, *et al*. Range-adaptive wireless power transfer based on differential coupling using multiple bidirectional coils. *IEEE Trans. Ind. Electron.* 2020, 67(9):7519–7528.

[30] Vital D, Bhardwaj S. Misalignment resilient anchor-shaped antennas in near-field wireless power transfer using electric and magnetic coupling modes. *IEEE Trans. Antennas Propag.* 2021, 69(5):2513–2521.

[31] Yang C, Chang C, Lee SY, Chang S, Chiou LY. Efficient four-coil wireless power transfer for deep brain stimulation. *IEEE Trans. Microwave Theory Tech.* 2017, 65(7):2496–2507.

[32] Di YJ, Gardner P, Hall PS, Ghafouri-Shiraz H, Zhou JF. Multiple-coupled microstrip hairpin-resonator filter. *IEEE Microwave and Wireless Compon. Lett.* 2003, 13(12):532–534.

[33] Kavitha R, Malarkodi B. Analysis of Impact of Bioimpedance on Performance of Implant Coil of Artificial Retina for Optimizing Q Factor & Bandwidth. *IEEE Trans. Biomed. Circuits Syst.* 2023, 17(1):142–151.

[34] Fadhel YB, AI-Haddad K. Wireless power transfer system using Helmholtz coils for powering Gastrointestinal Capsule biomedical implants. In *2024 21st International Multi-Conference on Systems, Signals & Devices (SSD)*, Erbil, Iraq, April 22–25, 2024, pp. 309–313.

[35] Zhang X, Lu J, Chen J, Tong L, Shi Y, *et al*. Impedance matching through a reconfigurable relay coil achieving maximum wireless power transfer under variations of coupling coefficient and load resistance. *IEEE Trans. Circuits Syst. I Regul. Pap.* 2024, 71(10):4851–4860.

[36] Kim J, Park S, Oh S, Huh Y, Cho J, *et al.* Cage-embedded crown-type dual coil wireless power transfer based microwave brain stimulation system for untethered and moving mice. *IEEE Trans. Biomed. Circuits Syst.* 2023, 17(2):362–374.

[37] Liu W, Ji Y, Wang W, Zhao Y, Wei Y. An out-tuned wireless power transfer system based machine learning for implantable medical devices. In *2023 3rd International Conference on Electrical Engineering and Mechatronics Technology (ICEEMT)*, Nanjing, China, 2023, pp. 867–871.

[38] Hossain ANMS, Mohseni P, Lavasani HM. Design and optimization of capacitive links for wireless power transfer to biomedical implants. *IEEE Trans. Biomed. Circuits Syst.* 2022, 16(6):1299–1312.

[39] Cai C, Chen T, Ren X, Jiao Y, Liu X, *et al*. Modeling and design of a transcutaneous resonant capacitive power transfer link for biomedical implants. *IEEE Trans. Power Electron.* 2025, 40(2):3726–3737.

[40] Pranta S, Barua N, Rahman MS, Salehin S, Alam SU, *et al.* Comprehensive analysis of RF-based wireless power transfer for enhancing implantable medical device performance. In *2024 IEEE International Conference on Biomedical Engineering, Computer and Information Technology for Health (BECITHCON)*, Dhaka, Bangladesh, November 28–29, 2024, pp. 35–38.

[41] Ma Y, Liu C, Huang Y, Ke H, Liu X. Combined magnetoelectric/coil receiving antenna for biomedical wireless power transfer. *IEEE J. Electromagn. RF Microwaves Med. Biol.* 2025, 9(1):15–26.

[42] Jing D, Li H, Ding X, Shao W, Xiao S. Compact and broadband circularly polarized implantable antenna for wireless implantable medical devices. *IEEE Antennas Wirel. Propag. Lett.* 2023, 22(6):1236–1240.

[43] Zhang J, Wagih M, Hoare D, Mirzai N, Mercer J, *et al*. Highly integrated and ultra-compact rectenna with wireless powering for implantable vascular devices. In *21st IEEE Interregional NEWCAS Conference (NEWCAS)*, Edinburgh, UK, June 26–28, 2023, pp. 1–5.

[44] Hosur S, Kashani Z, Karan SK, Priya S, Kiani M. MagSonic: hybrid magnetic-ultrasonic wireless interrogation of millimeter-scale biomedical implants with magnetoelectric transducer. *IEEE Trans. Biomed. Circuits Syst.* 2024, 18(2):383–395.

[45] Xu J, Filho JS, Nag S, Long L, Hwang E, *et al*. Fascicle-selective ultrasound-powered bidirectional wireless peripheral nerve interface IC. *IEEE Trans. Biomed. Circuits Syst.* 2023, 17(6):1237–1256.

[46] Sheng X, Lu D. High dynamic range class D power amplifier based on matching gain switching. In *2024 6th International Conference on Power and Energy Technology (ICPET)*, Beijing, China, July 12–15, 2024, pp. 229–233.

[47] Barbruni GL, Rodino F, Ros PM, Demarchi D, Ghezzi D, *et al.* A wearable real-time system for simultaneous wireless power and data transmission to cortical visual prosthesis. *IEEE Trans. Biomed. Circuits Syst.* 2024, 18(3):580–591.

[48] Sarkar S, Yao Y, Ki WH, Tsui CY. Hysteresis-dependent synchronized load shift keying and reconfigurable Class-D power amplifier-based fully integrated adaptive control in wireless power transfer system. *IEEE Trans. Circuits Syst. I Regul. Pap.* 2025, 72(5):2061–2074.

[49] Bai X, Lu Y, Zhan C, Martins RP. A 6.78-MHz wireless power transfer system with inherent wireless phase shift control without feedback data sensing coil. *IEEE J. Solid-State Circuits* 2023, 58(6):1746–1757.

[50] Liu Y, Yao Y, Ki WH. A 13.56-MHz single-input dual-output wireless power and data transfer system for bio-implants. *IEEE J. Solid-State Circuits* 2024, 59(8):2557–2567.

[51] Wang J, Lim EG, Leach MP, Wang Z, Pei R, *et al.* A 403 MHz wireless power transfer system with tuned split-ring loops for implantable medical devices. *IEEE Trans. Antennas Propag.* 2022, 70(2):1355–1366.

[52] Lu T, Makinwa KAA, Du S. A single-stage dual-output regulating voltage doubler for wireless power transfer. *IEEE J. Solid-State Circuits* 2024, 59(9):2922–2933.

[53] Lu T, Chang ZY, Jiang J, Makinwa K, Du S. A 13.56MHz fully integrated 91.8% efficiency single-stage dual-output regulating voltage doubler for biomedical wireless power transfer. In *2023 IEEE Custom Integrated Circuits Conference (CICC)*, San Antonio, USA, April 23–26, 2023, pp. 1–2.

[54] Luo Z, Liu J, Lee H. A 40.68-MHz active rectifier with cycle-based on-/off-delay compensation for high-current biomedical implants. *IEEE J. Solid-State Circuits* 2023, 58(2):345–356.

[55] Ahn J, Lee HS, Eom K, Jung W, Lee HM. A 13.56-MHz 93.5%-efficiency optimal on/off timing tracking active rectifier with digital feedback-based adaptive delay control. *IEEE Trans. Biomed. Circuits Syst.*, 2025, 19(3):562–576.

[56] Huang W, Zheng K, Liu X, Wang X, Hou Y, *et al.* Simultaneous high-efficiency power delivery and energy-efficient forward data transmission over single inductive link. *IEEE Access* 2023, 11:76793–76803.

[57] Lee HS, Eom K, Lee HM. 27.3 a 90.8%-efficiency SIMO resonant regulating rectifier generating 3 outputs in a half cycle with distributed multi-phase control for wirelessly-powered implantable devices. In *2024 IEEE International Solid-State Circuits Conference (ISSCC)*, San Francisco, USA, February 18–22, 2024, pp. 448–450.

[58] Zheng K, Hou Y, Wang X, Liu Y. A single-stage dual-output regulating rectifier with sequential pulse frequency modulation control for wireless biomedical applications. *IEEE Trans. Circuits Syst. II Express Briefs* 2024, 71(10):4566–4570.

[59] Chen S, Shi G, Liu X, Xu X, Wang B, *et al.* A single-stage 0X/1X regulating rectifier with improved voltage mode delay compensation for wirelessly powered implantable medical devices. *IEEE Access* 2024, 12:116114–116125.

[60] Fan H, Feng L, Diao X, Xie X, Wang C, *et al.* A fast transient LDO regulator featuring high PSRR over 100-kHz frequency range with adaptive, dynamic biasing, and current mode feed-forward amplifier. *IEEE Trans. Circuits Syst. II Express Briefs* 2024, 71(4):1764–1768.

[61] Sun Y, Zhang K, Wang J, An F, Fan X, *et al.* A fully integrated current-mode LDO using PSRC and APSR technique with –71.8 dB PSRR at 6.78 MHz for implantable medical device. In *2024 IEEE Biomedical Circuits and Systems Conference (BioCAS)*, Xi'an, China, October 24–26, 2024, pp. 1–5.

[62] Lee S, Lim J, Han J. A PSRR-enhanced fast-response inverter-based LDO for mobile devices. *IEEE Trans. Circuits Syst. II: Express Briefs* 2024, 71(6):3226–3230.

[63] Kim T, Kim B, Roh J. A 54-nA quiescent current capless LDO with −39-dB PSRR at 1 MHz using a load-tracking bandwidth extension technique. *IEEE Trans. Circuits Syst. II: Express Briefs* 2024, 71(3):1556–1560.

[64] Fan H, Feng L, Diao X, Xie X, Wang C, *et al.* A fast transient LDO regulator featuring high PSRR over 100-kHz frequency range with adaptive, dynamic biasing, and current mode feed-forward amplifier. *IEEE Trans. Circuits Syst. II: Express Briefs* 2024, 71(4):1764–1768.

[65] Karimi MJ, Dehollain C, Schmid A. Power feedback control unit for closed-loop wirelessly powered biomedical implants. *IEEE Trans. Circuits Syst. II: Express Briefs* 2023, 70(5):1674–1678.

[66] Zhang Q, Mai S, Zhou R, Yang X. A low-power ASK demodulator for wireless power and data transfer systems supporting ultra-low modulation depth of 0.03%. In *2023 IEEE International Symposium on Circuits and Systems (ISCAS)*, Monterey, USA, May 21–25, 2023, pp. 1–5.

[67] Karimi MJ, Zhou Y, Dehollain C, Schmid A. An analysis of an ASK demodulator with dual self-biased separated voltages for implantable applications. *IEEE Trans. Circuits Syst. II: Express Briefs* 2024, 71(6):2986–2990.

[68] Lee HS, Lee HM. A power-efficient envelope-detector-less amplitude-shift-keying forward telemetry for wirelessly powered biomedical devices. *IEEE Trans. Biomed. Circuits Syst.* 2025, 19(2):374–384.

[69] Zhao Z. Spectral efficiency comparison via implement different modulation schemes within ASK, FSK and PSK. In *13th International Conference on Information and Communication Technology (ICTech)*, Xiamen, China, April 12–14, 2024, pp. 366–371.

[70] Trigui A, Ali M, Ammari AC, Savaria Y, Sawan M. Quad-level carrier width modulation demodulator for micro-implants. In *2016 14th IEEE International New Circuits and Systems Conference (NEWCAS)*, Vancouver, Canada, June 26–29, 2016, pp. 1–4.

[71] Dhull P, Schreurs D, Paolini G, Costanzo A, Abolhasan M, *et al.* Multitone PSK modulation design for simultaneous wireless information and power transfer. *IEEE Trans. Microwave Theory Tech.* 2024, 72(1):446–460.

[72] Zhang X, Dai C, Yang C, Zhao Y, Zhang H, *et al.* A compact multi-channel neural stimulator with a high-efficiency wireless power and data transfer system for batteryless invasive BCIs. In *2024 IEEE Biomedical Circuits and Systems Conference (BioCAS)*, Xi'an, China, October 24–26, 2024, pp. 1–5.

[73] Qaragoez Y, Pollin S, Schreurs D. Biased-FSK modulation for simultaneous wireless information and power transfer. *IEEE Trans. Microwave Theory Tech.* 2024, 72(12):7071–7084.

[74] Karimi MJ, Jin M, Zhou Y, Dehollain C, Schmid A. Wirelessly powered and bi-directional data communication system with adaptive conversion chain for multisite biomedical implants over single inductive link. *IEEE Trans. Biomed. Circuits Syst.* 2024, 18(3):636–647.

[75] Dehghan K, Shoaei O, Jafarabadi Ashtiani S. A class-E power and data transmitter with improved data rate to carrier frequency ratio for medical implants. *IEEE Trans. Circuits Syst. II Express Briefs* 2022, 69(6):2692–2696.

[76] Yao D, Hung CC, Lo WP, Chen PH. A wireless-powered battery-less electrical stimulator with delay-shift keying (DSK) based downlink data communication. *IEEE Trans. Circuits Syst. I Regul. Pap.* 2024, 71(11):4900–4911.

[77] Park Y, Hung PD, Youn D, Kwon D, Kim C, *et al.* An enhanced-frequency-splitting-based wireless power and data transfer system achieving 60.2% end-to-end efficiency and 1 Mb/s data rate with a sub-cm RX coil for miniaturized implants. In *2025 IEEE International Solid-State Circuits Conference (ISSCC)*, San Francisco, USA, February 16–20, 2025, pp. 578–579.

[78] Lee HS, Ahn J, Kang M, Lee HM. A load-insensitive hybrid LSK back telemetry system with slope-based demodulation for inductively powered biomedical devices. *IEEE Trans. Biomed. Circuits Syst.* 2022, 16(4):651–663.

[79] Jung H, Lee B. Wireless power and bidirectional data transfer system for IoT and mobile devices. *IEEE Trans. Ind. Electron.* 2022, 69(11):11832–11836.

[80] Park Y, Koh ST, Lee J, Kim H, Choi J, *et al.* A frequency-splitting-based wireless power and data transfer IC for neural prostheses with simultaneous 115mW power and 2.5Mb/s forward data delivery. In *2021 IEEE International Solid-State Circuits Conference (ISSCC)*, San Francisco, USA, February 13–22, 2021, pp. 472–474.

[81] Trigui A, Ali M, Hached S, David JP, Savaria Y, *et al.* Generic wireless power transfer and data communication system based on a novel modulation technique. *IEEE Trans. Circuits Syst. I Regul. Pap*. 2020, 67(11):3978–3990.

[82] Cheng CH, Tsai PY, Yang TY, Cheng WH, Yen TY, *et al.* A fully integrated 16-channel closed-loop neuralprosthetic CMOS SoC with wireless power and bidirectional data telemetry for real-time efficient human epileptic seizure control. *IEEE J. Solid-State Circuits* 2018, 53(11):3314–3326.

[83] Qian XH, Wu YC, Yang TY, Cheng CH, Chu HC, *et al.* Design of a bone-guided cochlear implant microsystem with monopolar biphasic multiple stimulations and evoked compound action potential acquisition and its *in vivo* verification. *IEEE J. Solid-State Circuits* 2021, 56(10):3062–3076.

[84] Lee J, Kim Y, Kang D, Song I, Lee B. A reconfigurable bidirectional wireless power and full-duplex data transceiver IC for wearable biomedical applications. *IEEE Trans. Biomed. Circuits Syst.* 2025, 16(4):767–776.

[85] Yu Z, Zou Y, Liao HC, Alrashdan F, Wen Z, *et al.* A miniature batteryless bioelectronic implant using one magnetoelectric transducer for wireless powering and PWM backscatter communication. *IEEE Trans. Biomed. Circuits Syst.* 2024, 18(6):1197–1208.

[86] Saha N, Kakaraparty K, Pineda EA, Mahbub I. Wireless powering of implants and wearables: challenges (and opportunities) toward transitioning from bench-top to clinical studies [Bioelectromagnetics]. *IEEE Antennas and Propag. Mag.* 2025, 67(5):59–71.

[87] Zhang K, Liu CR, Jiang ZH, Zhang YD, Liu XG, *et al.* Near-field wireless power transfer to deep-tissue implants for biomedical applications. *IEEE Trans. Antennas Propag.* 2020, 68(2):1098–1106.

[88] Liu C, Zhang Y, Liu X. Circularly polarized implantable antenna for 915 MHz ISM-band far-field wireless power transmission. *IEEE Antennas Wireless Propag. Lett.* 2018, 17(3):373–376.

[89] Iqbal A, Sura PR, Al-Hasan M, Mabrouk IB, Denidni TA. Wireless power transfer system for deep-implanted biomedical devices. *Sci. Rep.* 2022, 12(1):13689.

[90] Zhu H, Yang H, Zhan L, Chen Y, Wang J, *et al.* Hydrogel-based smart contact lens for highly sensitive wireless intraocular pressure monitoring. *ACS Sens.* 2022, 7(10):3014–3022

[91] Gutruf P, Yin RT, Lee KB, Ausra J, Brennan JA, *et al.* Wireless, battery-free, fully implantable multimodal and multisite pacemakers for applications in small animal models. *Nat. Commun.* 2016, 10(1):5742.

[92] Chen L, Tee BC, Chortos AL, Schwartz G, Tse V, *et al.* Continuous wireless pressure monitoring and mapping with ultra-small passive sensors for health monitoring and critical care. *Nat. Commun.* 2014, 5(1):5028.

[93] Kim JH, Lee SJ, Jeong YW, Cho MJ, Kim MS, *et al.* A programming-free three-dimensional resonant current-mode wireless receiver with real-time link-adaptivity and a 0.904 cm^3 receiver coil for implantable systems. In *2025 IEEE International Solid-State Circuits Conference (ISSCC)*, San Francisco, USA, February 16–20, 2025, pp. 580–581.

[94] Bennia F, Boudouda A, Nafa F. Optimal design of wireless power transfer coils for biomedical implants using machine learning and meta-heuristic algorithms. *Electr. Eng.*, 2024, 106(5):5869–5884.

[95] Zhang H, Liao M, He L, Lee CK. Parameter optimization of wireless power transfer based on machine learning. *Electronics* 2023, 13(1):103.

[96] Jeong S, Lin TH, Tentzeris MM. Range-adaptive impedance matching of wireless power transfer system using a machine learning strategy based on neural networks. In *IEEE MTT-S Int. Microw. Symp. Dig.*, Boston, USA, June 2–7, 2019, pp.1423–1425.

[97] Srivastava VK, Ahmad A, Sharma A. A machine-learning-assisted localization and magnetic field forming for wireless powering of biomedical implant devices. *IEEE Trans. Antennas Propag.* 2024, 72(11):8590–8599.

[98] Liu W, Ji Y, Wang W, Zhao Y, Wei Y. An out-tuned wireless power transfer system based machine learning for implantable medical devices. In *2023 3rd International Conference on Electrical Engineering and Mechatronics Technology (ICEEMT)*, Nanjing, China, July 21–23, 2023, pp. 867–871.

[99] Gong Y, Otomo Y, Igarashi H. Sensorless metal object detection for wireless power transfer using machine learning. *COMPEL-Int. J. Comput. Math. Electr. Electron. Eng.* 2022, 41(3):807–823.

[100] Rajamanickam N, Abraham DS, Alroobaea R, Abdelfattah WM. Foreign object debris detection on wireless electric vehicle charging pad using machine learning approach. *Processes* 2024, 12(8):1574.